ACS OMEGA

http://pubs.acs.org/journal/acsodf

Article

Waste Valorization of a Recycled ZnCoFe Mixed Metal Oxide/Ceftriaxone Waste Layered Nanoadsorbent for Further Dye Removal

Yasser GadelHak, Esraa Salama, Samah Abd-El Tawab, Eman Abouzied Mouhmed, Dalal Hussien M. Alkhalifah, Wael N. Hozzein, Mona Mohaseb, Rehab K. Mahmoud,* and Rafat M. Amin

Cite This: *ACS Omega* 2022, 7, 44103−44115

Read Online

ACCESS | Metrics & More | Article Recommendations

ABSTRACT: Waste valorization of spent wastewater nanoadsorbents is a promising technique to support the circular economy strategies. The terrible rise of heavy metal pollution in the environment is considered a serious threat to the terrestrial and aquatic environment. This led to the necessity of developing cost-effective, operation-convenient, and recyclable adsorbents. ZnCoFe mixed metal oxide (MMO) was synthesized using co-precipitation. The sample was characterized using X-ray powder diffraction, Fourier transform infrared spectroscopy, and scanning electron microscopy. Factors affecting the adsorption process such as pH, the dose of adsorbent, and time were investigated. ZnCoFe MMO showed the maximum adsorption capacity of 118.45 mg/g for ceftriaxone sodium. The spent MMO was recycled as an adsorbent for malachite green (MG) removal. Interestingly, the spent adsorbent showed 94% removal percent for MG as compared to the fresh MMO (90%). The kinetic investigation of the adsorption process was performed and discussed. In addition, ZnCoFe MMO was tested as an antimicrobial agent. The proposed approach opens up a new avenue for recycling wastes after adsorption into value-added materials for utilization in adsorbent production with excellent performance as antimicrobial agents.

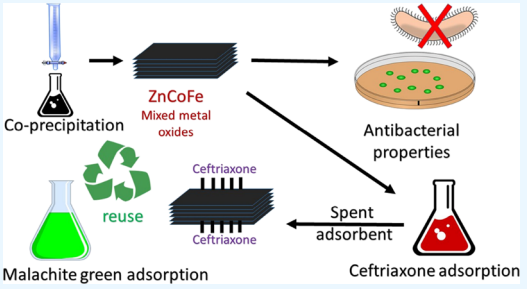

1. INTRODUCTION

Achieving circular economy requires much effort to implement reuse and valorization strategies for different types of wastes including solid wastes for the production of higher value products.[1,2] Industrial activities are the source of many waste products such as spent adsorbents, exhausted or poisoned catalysts, wastewater effluents, and air pollutants. The concept of reusing spent adsorbents is gaining attention in recent years. In a recent review, Baskar et al.[3] discussed the different routes for the regeneration and sustainable management of spent adsorbents. One of these routes is soil amendment where nutrients recovered from agriculture wastewater can be reused to improve the fertility of the soil. Other management strategies include using the adsorbents as catalysts, capacitors, catalyst supports, sensors, and cement additives. In another recent review, Rial and Ferreira[4] further detailed numerous uses for spent wastewater adsorbents. The authors cited several studies that successfully reused spent adsorbents as catalysts, as construction material fillers, as components in industrial products, and in further environmental remediation applications. This last strategy is a promising one since it allows the same adsorbent to be further used to remove more pollutants from wastewater streams while still showing high performance in terms of removal efficiency and capacity.

Few studies are available in the open literature reporting the reuse of spent layered double hydroxides (LDHs) or the corresponding mixed metal oxide (MMO) adsorbents in the field of further environmental remediation. LDHs are two-dimensional (2D) anionic clay materials with a structure similar to brucite and chemical formula $[M(II)(1-x)M(III)x(OH)2]^{x+}(A^{n-})_{x/n}{\cdot}yH_2O$. M(II) is a divalent cation such as Mg, Ni, Zn, Cu, or Co and M(III) is a trivalent cation such as Al, Cr, Fe, or Ga, while A^{n-} is negative anions such as CO_3^{-2}, Cl^-, NO_3^-, or organic anions.[5] LDHs have attracted much interest in recent years as adsorbents due to having large specific surface area, low toxicity, high anion substitution capacity, ease of recoverability, economic production, and high stabilities for chemical and thermal properties.[6] Laipan et al.[7] prepared a CuFe LDH using a simple coprecipitation method and used it as an adsorbent for oil as a model organic contaminant. Upon thermal treatment in an inert atmosphere, the sample was converted into zero valent Cu and Fe

Received: August 27, 2022
Accepted: November 8, 2022
Published: November 17, 2022

supported on carbon. This produced material was further used for Cr(VI) removal by adsorption. The carbonaceous adsorbent showed specific surface areas from 141−744 m^2/g and a removal capacity of around 60 mg/g. Shen et al.[8] followed a similar approach where ZnAlLa LDH was used as an adsorbent for the azo food colorant amaranth. However, after thermal calcination, the resultant carbonaceous material was used as a photocatalyst for the degradation of ibuprofen. Still much work is needed to investigate the reuse and valorization of waste spent LDH-based adsorbents.[9]

Our research group has contributed to this research field through exploring novel techniques to reuse and/or valorize spent adsorbents. Moustafa et al.[10] reported the successful reuse of spent ZnFe LDH nanoadsorbents, after being used for methyl orange (MO) adsorption, as a methylene blue (MB) adsorbent. Abdel-Hady et al.[11] followed a different approach where ZnCoFe LDH was used as a nanoadsorbent for MB adsorption. To follow, the spent adsorbent was tested as a direct methanol electro-oxidation catalyst. The authors reported a maximum current density of 41.11 mA/cm^2 (50 mV/s and methanol concentration = 3 M). In addition, Abdel-Hady et al. (under publication) reported preparing double substituted CoNiZnFe LDH as a nanoadsorbent, and the corresponding MMO calcined at different temperatures (200, 400, and 600 °C). The spent adsorbents after MO adsorption were used an electrocatalyst for direct methanol electro-oxidation showing a maximum current density of 6.46 and 10.1 mA/cm^2 for the LDH sample and the MMO sample calcined at 200 °C, respectively.

The aim of the current work is to investigate ZnCoFe MMO as a 2D layered nanoadsorbent for ceftriaxone sodium (CTX) removal from wastewater. ZnCoFe MMO was characterized using X-ray powder diffraction (XRD), Fourier transform infrared (FTIR) spectroscopy, and scanning electron microscopy (SEM). The effect of solution pH, adsorbent dosage, CTX initial concentration, adsorption kinetics, and temperature were studied. The spent adsorbent was further valorized as an adsorbent for the removal of malachite green (MG) dye from simulated wastewater. Finally, the antimicrobial activity of ZnCoFe MMO was tested as illustrated in Scheme1.

Scheme 1. Procedure of Reusing ZnCoFe MMO Spent Adsorbent for MG Adsorption

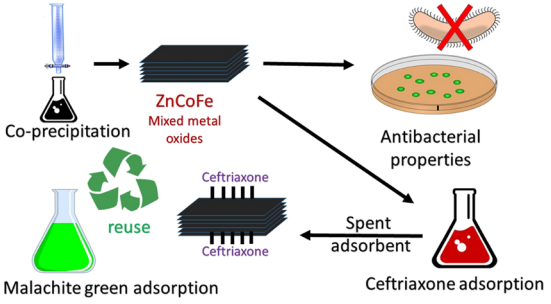

As listed in Table 1, a comparison of the prepared material with other adsorbents was conducted. To further estimate the importance of the prepared materials for wastewater remediation from CTX, the maximum adsorption capacity (q_{max}) obtained was carefully compared to other adsorbents. By analyzing the value of adsorption capacity, it seems that the as-prepared MMO can be a potentially effective material for use in CTX-polluted aquatic systems. Also, a comparison was performed for MG uptake using different materials. The reused spent MMO/CTX adsorbent seems to be a promising material for MG adsorption from wastewater streams. This study opens up a new avenue for recycling waste adsorbents after adsorption into value-added materials. Such reused materials can be further utilized as adsorbents showing excellent performance and multifunctionality as antimicrobial agents as well.

2. MATERIALS AND METHODS

2.1. Materials. Zinc nitrate (Chem-Lab NV-Belgium), cobalt nitrate, and ferric nitrate (Oxford-India) were used as received without any further purification. Sodium hydroxide (NaOH) was purchased from Egyptian Piochem for laboratory chemicals. CTX was used as an adsorbate in the recent study (Table 2). Hydrochloric acid (HCl) was purchased from CarloErba reagents (Egypt). Methanol was supplied from ALPHA CHEMIKA (India). MG $C_{23}H_{25}N_2Cl$ was purchased from LABAL Chemie (India). All chemicals are at a high standard of analytical grade.

2.2. Synthesis of ZnCoFe MMO. The co-precipitation method was used to prepare ZnCoFe LDHs following a procedure similar to our previous work.[24] The ratio of Zn nitrate to cobalt nitrate to ferric nitrate used was adjusted to be 1.5:1.5:1, respectively. Briefly, metal nitrates were precipitated using a slow addition (0.1 mL/min) of NaOH solution (2 M) until the solution pH reached 9 to assure complete precipitation of the corresponding metal hydroxides. To follow, the precipitated hydroxides were left under continuous stirring overnight to age. The formed suspension was then filtered and washed using distilled water and finally washed with ethanol. Finally, the resulting powder was dried for 1 day at 80 ± 0.5 °C as a mild thermal oxidation process to obtain the corresponding layered MMOs.

2.3. Material Characterization. The prepared ZnCoFe MMO was characterized using different tools: PANalytical (Empyrean) X-ray diffractometer with Cu-Kα radiation (wavelength 0.154 nm, current = 35 mA, voltage = 40 kV, scanning at rate of 8° min^{-1}) from two-theta of 5 to 80° was used to determine the crystallinity of the sample. The functional groups were determined using FTIR spectroscopy (Bruker-Vertex 70, KBr pellet technique, Germany), from 400 to 4000 cm^{-1} wavenumber. The microstructure and morphology of the synthesized ZnCoFe MMO were investigated using field emission scanning electron microscope. CTX and MG concentrations were measured using a UV−vis spectrophotometer (SHIMADZU UV-2600). Atomic absorption spectroscopy (AAS) (model ZEISS-AA55, Germany) was used to detect the concentrations of elements in solutions.

2.4. Adsorption Study. Experiments for the adsorption study were performed in a batch mode at ambient temperature (25 °C). A standard stock solution (for CTX and MG) of a concentration 1000 mg/L was prepared to allow series dilution to obtain less concentrated solutions for the calibration curve (5−500 mg/L). To study the effect of pH, six 50 mL Falcon tubes were filled with 50 mg/L solution and 0.05 g of the synthesized ZnCoFe MMO adsorbent was added. The pH was adjusted using 0.1 M NaOH or 0.1 M HCl to the required value which was tracked using a pH meter (Metrohm 751 Titrino). The tubes were then placed on an orbital shaker (SO330-Pro) overnight until reaching equilibrium. Samples were collected using a syringe equipped with a (Millipore,

https://doi.org/10.1021/acsomega.2c05528
ACS Omega 2022, 7, 44103−44115

Table 1. Recent Studies Reporting the Adsorption of CTX and MG Compared to the Current Study

adsorbent	adsorbate	pH	adsorbate concentration (mg/L)	equilibrium time (min)	adsorbent mass (g)	removal percent	Q_{max} (mg/g)	reference
ZnCoFe MMO	CTX	7	50	60	0.05	85%	322	(This work)
TiO_2/chitosan/nanobentonite	CTX	5	25	10	2	93.5%	90.9	12
Pseudomonas putida biomass	CTX	7	50	120	0.1	50%	109.5	13
C_3N_4/ multiwalled carbon nanotube /Bi_2WO_6	CTX	4	50	10	0.015	98.4%	19.6	14
Fe_3O_4/activated carbon	CTX	3	10	90	1.99	97.1%	28.9	15
ZnCoFe/CTX ZnCoFe MMO	MG	7	50	10	0.005	94% 90%	34.2 23.3	(This work)
MgAl LDH/Biochar	MG		25	150	2	66.7%	70.9	16
activated carbon	MG	4	100		0.1	22%	115	17
Fe-BTC metal−organic frameworks	MG	4	1.5 (mM)	30	0.1	98.5%	177	18
ZIF-8@Fe/Ni	MG	4.5	50	120	0.5	92%	151.5	19

Table 2. Physical and Chemical Properties of CTX[20−23]

IUPAC name	disodium;(6R,7R)-7-[[(2Z)-2-(2-amino-1,3-thiazol-4-yl)-2-methoxyiminoacetyl]amino]-3-[(2-methyl-6-oxido-5-oxo-1,2,4-triazin-3-yl)sulfanylmethyl]-8-oxo-5-thia-1-azabicyclo[4.2.0]oct-2-ene-2-carboxylate
Molecular Formula	$C_{18}H_{16}N_8Na_2O_7S_3$
Molecular weight	598.6 g/mol
pK_a	~3 (COOH), 3.2 (NH_3^+), 4.1 (enolic OH)
colour	White to Off-White
Molecular structure	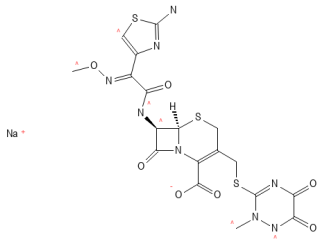

Nylon, 0.22 mm pore size) syringe filter and the residual concentration was measured using UV−vis spectroscopy.

The amount of CTX adsorbed (q_e) and removal percentage (%R) were calculated according to the following equations, respectively:

$$q_e = \frac{(C_o - C_t)V}{W} \quad (1)$$

$$\text{Removal percent } (\%R) = \frac{C_o - C_t}{C_o} \times 100 \quad (2)$$

where q_e is the amount of CTX adsorbed per gram, C_o and C_t are the initial concentration and the concentration after adsorption of CTX in (mg/L) at time t (min), respectively, W is the weight of adsorbent in grams, and V is the volume of CTX solution (Liter).

The effect of adsorbent dosage was studied at a constant concentration of CTX (50 mg/L) while the amount of adsorbent varied from 0.0125 to 0.10 g. Moreover, the effect of CTX initial concentration was studied at a constant adsorbent weight (0.075 g) representing the optimum condition of the dose of the adsorbent. Different CTX initial concentrations were used ranging from 5 to 500 mg/L. To follow, two-, three-, and four-parameter isotherm models have been applied to fit the adsorption data. In addition, the effect of temperature on the adsorption process was examined at temperatures of 15, 25, 35, 45, and 55 °C and the corresponding thermodynamic parameters were calculated. Finally, adsorption kinetics were studied and data were fitted to numerous kinetic models such as pseudo-first-order,[25] pseudo-second-order,[26] intraparticle diffusion,[27] and Avrami[28] at different time intervals ranging from 0 to 240 min. It should be mentioned that every adsorption experiment was performed in triplicate.

2.5. Novel Recycling, Collecting of Spent MMO for Further Applications. After the removal of CTX, the spent MMO powder was collected, washed, and then dried for 1 day at 80 ± 0.5 °C for the investigation of the further removal of MG.

2.6. Batch Adsorption Tests of MG by MMO and MMO/CTX. The adsorption experiments were carried out under shaking in dark conditions throughout the test at ambient temperature. Samples were withdrawn from the tested solution at appropriate time intervals and centrifuged (8000 rpm) for 3 min. The concentration of MG dye in the supernatant solution was measured using a UV−vis spectrophotometer (UV 1800, Shimadzu, Japan) at a wavelength of 617 nm as the maximum wavelength of MG dye. It should be

https://doi.org/10.1021/acsomega.2c05528
ACS Omega 2022, 7, 44103−44115

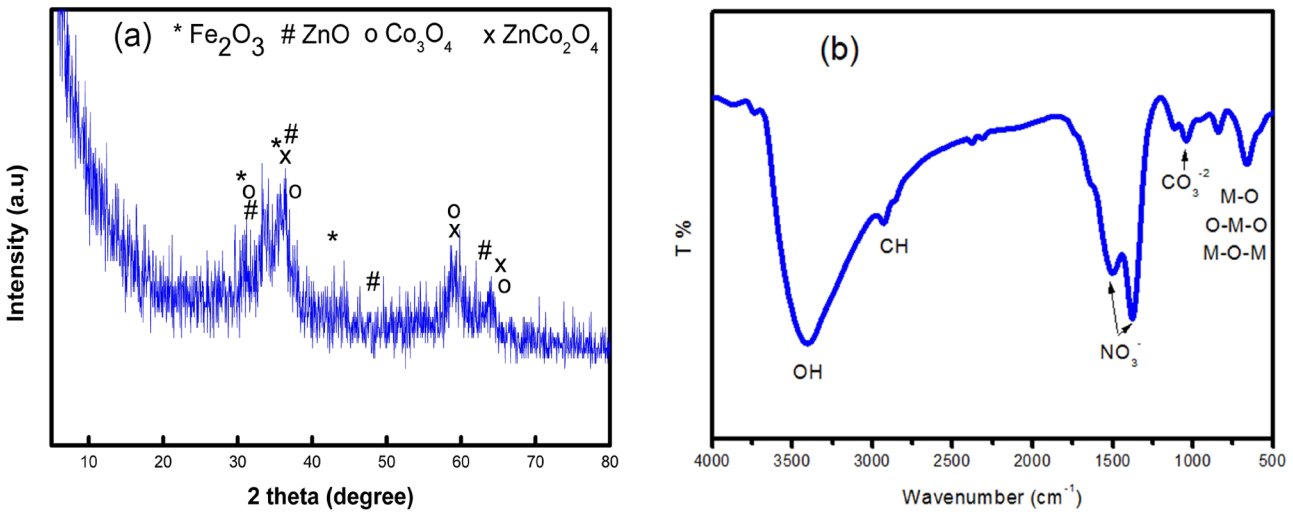

Figure 1. (a) XRD and (b) FTIR of the prepared ZnCoFe MMO nanoadsorbent.

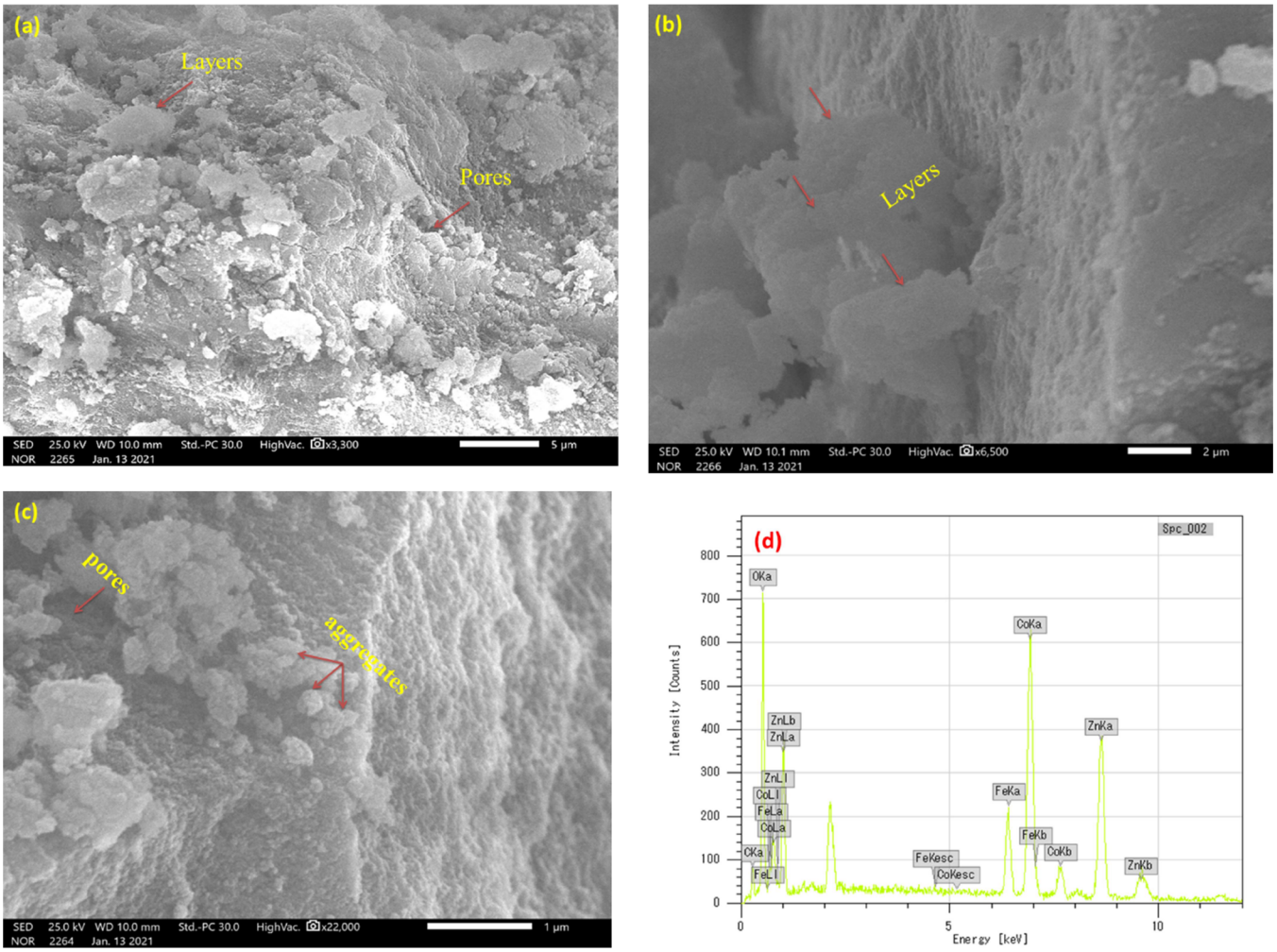

Figure 2. (a–c) SEM images with different magnifications, and (d) EDX spectrum of the prepared material ZnCoFe MMO.

mentioned that every adsorption experiment was performed in triplicate.

2.7. Estimation of the Antimicrobial Activity. *2.7.1. Indicator Microorganisms.* Gram-negative bacteria (*Escherichia coli* ATCC 25922) and Gram-positive bacteria (*Staphylococcus aureus* ATCC 8095) were used as indicator bacteria for the investigation of the antibacterial activity of the MMO adsorbent. All strains mentioned above were obtained from the culture collection of Agricultural Microbiology Department, Faculty of Agriculture, Fayoum University.

2.7.2. Antibacterial Activity Study Using the Well Diffusion Method. The antimicrobial activity of Zn/Fe/Co

https://doi.org/10.1021/acsomega.2c05528
ACS Omega 2022, 7, 44103−44115

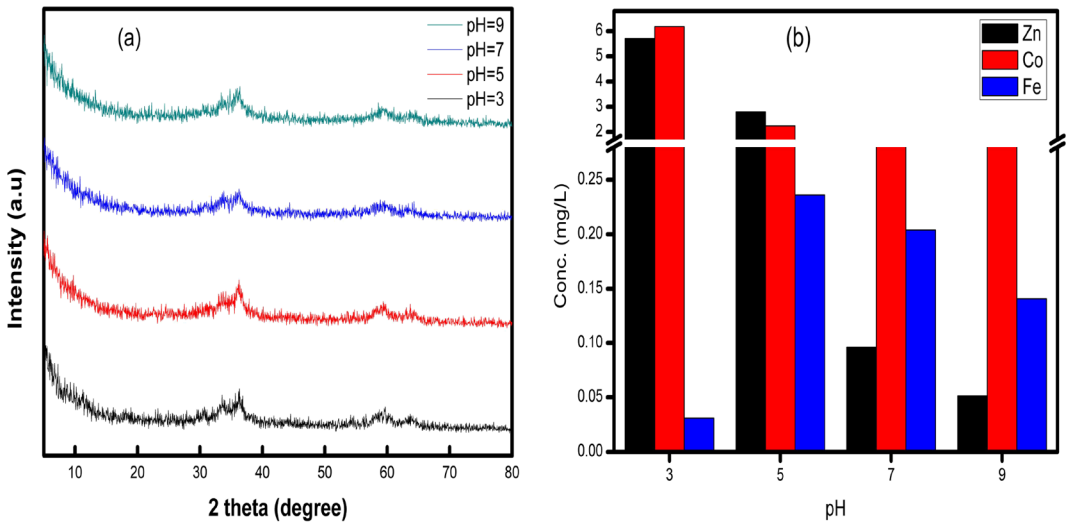

Figure 3. Assessment of stability of ZnCoFe MMO at different pH values: (a) XRD diffractograms and (b) AAS for Zn, Co, and Fe metal ion concentration.

LDH against Gram-positive (*S. aureus*) and Gram-negative (*E-coli*) bacteria was tested using the well diffusion method in the presence of Draxxin (92.9%) as a standard drug as reported in ref 29, 30. In Luria broth, stock cultures of the studied bacteria were cultivated for 18 h. Using the McFarland solutions standards, final cell concentrations were standardized till 10^7−10^8 cfu/mL.[31] This inoculum was added in a 1 mL to a plate of Luria Bertani Agar. Two wells (6 mm in diameter) formed in each plate as the agar solidified. Each well received 100 μL from concentrations 5, 50, 75, and 100 mg/mL of ZnFeCo MMO, suspended in distilled water. The plates were inoculated at 37 °C for 48 h following a diffusion period of 12−15 min at room temperature. The inhibition diameter was then calculated in millimeters. This experiment was repeated three times.

2.7.3. Determination of Minimum Inhibitory Concentration. According to the Natural Committee for Clinical Laboratory (NCCLS 1999) Standard's recommendation, a microdilution broth susceptibility test was conducted. The concentrations of 1, 5, 10, 20, and 30 mg/mL were tested for ZnFeCo MMO. These quantities were added to 1-mL nutrient broth tubes that contained live microorganisms at a density of 10^6 cfu/mL. To spread the sample throughout the broth, tubes were incubated in a shaking incubator. The minimum inhibitory concentration (MIC) was defined as the lowest concentration (maximum dilution) that showed no discernible increase. To determine if the inhibition was irreversible or permanent, cells from the tubes that showed no growth were subcultured on NA plates, and every test was performed by in duplicate.

3. RESULTS AND DISCUSSION

3.1. ZnCoFe MMO Sample Characterization. The XRD diffractogram of ZnCoFe MMO is illustrated in Figure 1a. As shown, several oxides could be detected such as Fe_2O_3, ZnO, Co_3O_4, and $ZnCo_2O_4$. The main peaks for these oxides overlap and due to the semicrystalline nature of the powder, it can be challenging to distinguish each separate phase. ZnO peaks could be detected at two theta values of 31.7, 36.2, 47.6, and 62.9° which is similar to previously reported data for Wurtzite (JCPDS No. 36-1451).[32] Fe_2O_3 showed peaks at 30.2, 35.6, and 43.3° (JCPDS-39-1346).[33] Co_3O_4 showed peaks at 31.3, 36.9, 59.4, and 65.2°,[34] while $ZnCo_2O_4$ showed diffraction peaks at 36.9, 59.3, and 65.2°.[35]

The FTIR spectrum of the ZnCoFe MMO sample (Figure 1b) shows a broad peak around 3400 cm^{-1}, which can be ascribed to the hydroxide ions stretching originating from adsorbed water molecules.[24,36] Two sharp peaks at around 1510 and 1368 cm^{-1} can be attributed to the stretching mode of the nitrate ions.[11] The small peak at around 2900 cm^{-1} may originate from ethanol molecules used during the washing step.[37] Probably, both the nitrate ions and ethanol molecules were trapped in the interlayer spacing between LDH layers and could not escape during the mild calcination process to obtain the MMO sample. The peaks below 1000 cm^{-1} can be attributed to the metal oxide (M−O, O−M−O, and M−O−M) bond absorption where M is the metal (Zn, Co, or Fe).[38,39]

SEM images of the prepared ZnCoFe MMO are shown in Figure 2. Figure 2a shows that the sample is in the form of a layered structure. Figure 2b shows a close up on the layered structure of the sample showing that the layers have an approximate diameter of 3 μm. Figure 2c shows that the sample contains some aggregated particles which may be in the form of very small layers. The difference in layer sizes can be attributed to the co-precipitation method for the preparation of the original ZnCoFe LDH, which lacks control over the layer size. Figure 2d shows the EDX spectra illustrating the pure nature of the sample with no signals other than Zn, Co, and Fe signals.

Figure 3a shows the XRD diffractograms of the ZnCoFe MMO sample after being immersed in solutions with different pH values. The XRD data show that the sample preserves the main diffraction peaks indicating the stability of the MMO structure irrespective of the pH value. AAS was further used to assess the chemical stability of ZnCoFe MMO by calculating the concentration percentages of zinc, cobalt, and iron in solution at various starting pH values (3−9) as shown in Figure 3b. This figure indicates that even though the MMO preserves its structure at different pH values (as discussed before), the chemical composition of the MMO sample can change. This is possibly due to the leaching of divalent and

https://doi.org/10.1021/acsomega.2c05528
ACS Omega 2022, 7, 44103−44115

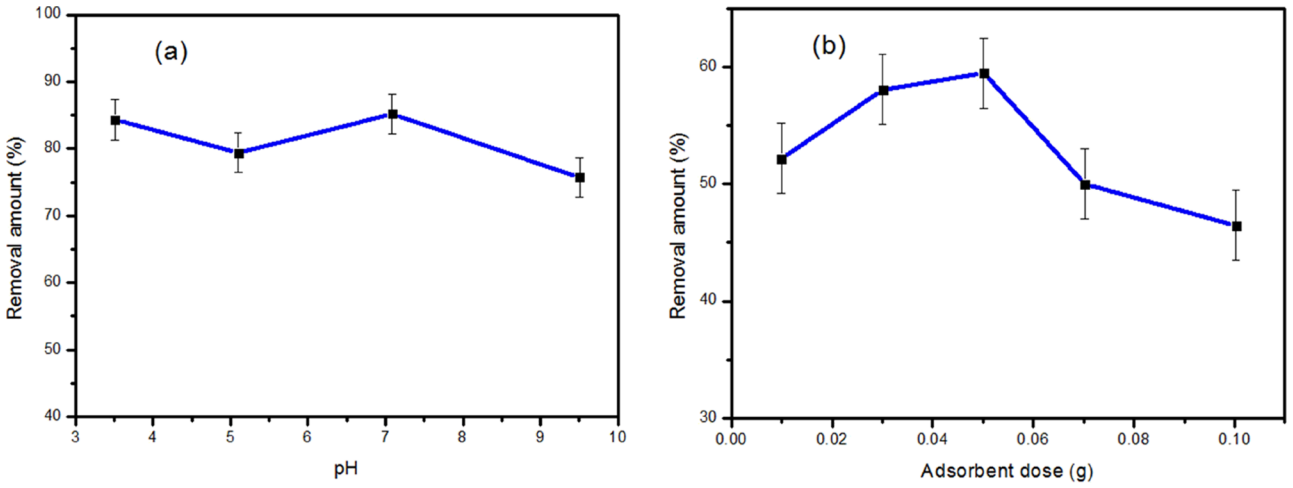

Figure 4. Effect of (a) pH and (b) adsorbent dose on the adsorption of CTX on ZnCoFe MMO.

Table 3. Nonlinear Adsorption Isotherm Models Using ZnCoFe MMO as the Adsorbent

isotherm models	expression	adjustable model parameters*	values	R^2
	Two-Parameter Isotherm			
Langmuir	$q_e = \frac{q_{max} K_L C_e}{1 + K_L C_e}$ q_{max} is a parameter that reflects monolayer formation, K_L is the adsorption equilibrium constant	q_{max} (mg/g) K_L (L/mg)	322 1.80×10^{-3}	0.98
Freundlich	$q_e = K_f C_e^{1/n_f}$ K_f is a constant for the relative adsorption capacity, $1/n_f$ is a constant indicative of surface heterogeneity	K_f (L/g) $1/n_f$ (−)	1.9 0.71	0.97
D-R	$q_e = (q_m) \exp. (-K_{ad} \varepsilon^2)$ $\varepsilon = RT (1 + (1/C_e))$ K_{ad} is a constant related to adsorption energy, q_m is the theoretical adsorption capacity.	q_m (mg/g) K_{ad} (mol^2/kJ^2)	231 0.036	0.99
	Three-Parameter Isotherm			
Langmuir–Freundlich	$q_e = \frac{q_{max} (K_{LF} C_e)^{\beta_{LF}}}{1 + (K_{LF} C_e)^{\beta_{LF}}}$ q_{max}, K_{LF} and β_{LF} are the max. adsorption capacity, the equilibrium constant, and the heterogeneity parameter, respectively.	q_{max} (mg/g) K_{LF} (L/mg) β_{LF} (−)	199 0.5×10^{-2} 1.84	0.99
Sips	$q_e = \frac{q_{max} K_S (C_e)^{n_s}}{1 + K_S (C_e)^{n_s}}$ q_{max}, K_S and n_s are the Sips max. adsorption capacity, equilibrium constant, and the model exponent, respectively	q_{max} (mg/g) K_s (L/mg) n_s (−)	196 4.90×10^{-5} 1.84	0.99
Redlich–Peterson	$q_e = \frac{q_{max} C_e}{1 + K_S (C_e)^{\beta_s}}$ q_{max}, K_s and β_s are the isotherm constants	q_{max} (L/mg) K_s (mg/g)^g β_s (−)	0.47 7.8×10^{-7} 2.12	0.99
Toth	$q_e = \frac{K_e C_e}{[1 + (K_L C_e)^n]^{1/n}}$ K_e, K_l, and n are Tóth max. adsorption capacity, Tóth equilibrium constant, and Tóth model exponent, respectively	K_e (mol*L/mg*mg) K_L (L/mg) n (−)	0.86 6.90×10^{-6} 1.79	0.99
	Four-Parameter Isotherm			
Baudu	$q_e = \frac{q_{max} b_o (C_e)^{1+x+y}}{1 + b_o (C_e)^{1+x}} q_{max}$ and b_o are the Baudu max. adsorption capacity and the equilibrium constant, respectively, x and y are the Baudu parameters	q_{max} (mg/g) b_o (−) X (−) Y (−)	171 5.17×10^{-5} 19.7×10^{-3} 8.45×10^{-1}	0.99

trivalent ions from the structure depending on the acidity or basicity of the solution.

3.2. ZnCoFe MMO Adsorption Study. *3.2.1. Effect of pH and Adsorbent Dosage.* In general, pH is one of the most important factors affecting the adsorption of adsorbates onto the surface of materials due to the electrostatic interaction. The effect of pH of a solution on CTX adsorption onto ZnCoFe MMO is shown in Figure 4a. As shown, in the acidic range of pH till pH = 7, no significant variation could be measured in the value of the removal amount of CTX on ZnCoFe MMO. At pH = 7, the zeta potential of ZnCoFe LDH was calculated to be 27 mV. In addition, in acidic media, ZnCoFe LDH has a positive charge[11] which is similar to the parent ZnFe LDH that has a positive zeta potential in acidic media.[6] On the other hand, CTX has three dissociation constants at $pK_1 = 3$, $pK_2 = 3.2$, and $pK_3 = 4.1$.[40] Therefore with increasing pH value above pK_a, CTX will acquire a negative charge[41] leading to electrostatic repulsion with the MMO surface. The insignificant decrease in the value of the removal amount shows that there may be other adsorption mechanisms responsible for CTX adsorption irrespective of the possible electrostatic repulsion. At basic pH (pH > 7), the dominance of OH ions in solution generates a competition with CTX on the adsorption process on the MMO surface[42] leading to the decrease of the measured removal amount.

https://doi.org/10.1021/acsomega.2c05528
ACS Omega 2022, 7, 44103−44115

Figure 4b shows the results for the removal efficiency of CTX with ZnCoFe MMO. A dose of 0.01 to 0.10 g was used per 10 mL of CTX diluted solution at pH 7. The removal efficiency of CTX increased to 59% with an increase in the amount of ZnCoFe MMO up to 0.04 g, which may be attributed to more accessible active sites for adsorption. However, the removal efficiency of CTX was reduced to 46.50% when the dose of MMO was up to 0.10 g. This could be because the aggregation of MMO particles occurs.[43]

Under the optimum solution pH conditions, at solution pH 7, the charge of the partials was positive (27 mV), and the high hydrophobicity, with increase in the amount of adsorbent and enhanced van der Waals force interaction, causes the MMO to aggregate.[44−46] The origin of van der Waals like attraction is induced dipoles, a bulk material with an electronic or molecular structure that favors the generation of permanent or formed dipoles that promote aggregation. Also, interaction of the adsorbent surfaces with water molecules involves a significant entropic penalty driving an aggregation process that may have occurred.[47]

3.2.2. Effect of Initial Concentration. Several equilibrium isotherm models were tested to fit the experimental data of using ZnCoFe MMO as an adsorbent. The models used were Langmuir,[48] Freundlich,[49] Dubinin−Radushkevich (D-R),[50] Langmuir−Freundlich and Sips,[51] Redlich−Peterson,[52,53] Toth,[54] and Baudu[55] isotherm. The results demonstrated that the Langmuir model is the most adequate in the case of ZnCoFe MMO because it showed the highest adsorption capacity with the highest R^2 value of 0.98 as illustrated in Table 3. ZnCoFe MMO as an adsorbent for the adsorption of CTX from an aqueous solution showed a maximum adsorption capacity (q_{max}) of 322 mg/g for CTX as shown in Figure 5. Similar results were obtained for different adsorbent-pollutant systems in the literature.[56−58]

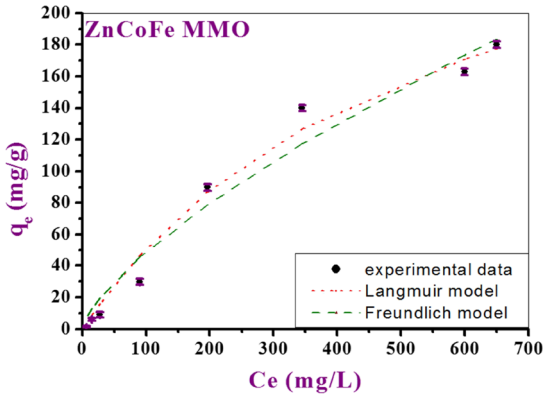

Figure 5. Experimental adsorption isotherm data of CTX on the prepared MMO fitted using the two-parameter isotherm models as a representative model.

3.2.3. Adsorption Kinetics. From the experimental data, it is obviously clear that the uptake efficiency of CTX onto the MMO increases rapidly during the early time of adsorption due to the existence of the vacant active centers, till the time interval of 10 min (Figure 6). After 10 min, the equilibrium state was reached. The adsorption process was best fitted with pseudo-first-order, pseudo-second-order, 1,2 mixed order, and Avrami models, with high R^2 values as shown in Table 4. The kinetics of adsorption results of CTX on MMO was best fit with the pseudo-second-order model. In this model, the

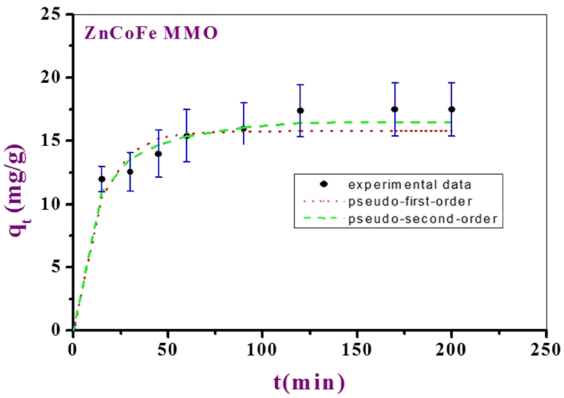

Figure 6. Kinetic modeling of CTX adsorption on MMO.

removal CTX from a solution is due to chemical adsorption interactions between the two phases.[59]

3.2.4. Effect of Temperature. The temperature is a very important parameter that affects the adsorption process. The influence of temperature was investigated at the optimum conditions (0.05 g dose of adsorbent per 50 mL, 50 mg/L concentration of CTX, pH = 7.00 till equilibrium) at various temperatures: 25−55 °C. The results show an inverse relation between the removal efficiency and the temperature due to the physical adsorption which is an exothermic process (desorption occurs with the increase of temperature) according to Le Chatelier's principle.[60] Such an inverse relation might occur due to the weakness of the bonding between CTX and the synthesized adsorbents.[61,62] Thermodynamic analysis was performed in terms of Gibb's free energy change (ΔG°), enthalpy change (ΔH°), and entropy change (ΔS°), which were calculated using the results of the preinvestigated experiments (Table 5) and the values of $K_d = (q_e/C_e)$ were also calculated at various temperatures using the van't Hoff equation to determine the mechanism of the adsorption process.[63]

$$\ln K_d = \Delta S^\circ/R - \Delta H^\circ/RT \quad (3)$$

where K_d is the equilibrium constant (L/mg), ΔH° is the enthalpy change of adsorption (kJ/mol), R: is the gas constant (8.314 J/mol K), and ΔS° is the entropy change of adsorption. ΔS° was calculated from the intercept and the slope of the straight-line plot of ln K_d versus $1/T$ (K^{-1}).

Gibbs free energy change (ΔG°) could be obtained using eqs 4 and 5.

$$\Delta G^\circ = -RT \ln K_d = \Delta H^\circ - T\Delta S^\circ \quad (4)$$

$$\ln K_d = -\Delta H^\circ/R(1/T) + \Delta S^\circ/R \quad (5)$$

As shown in Figure 7, the plot of ln K_d versus $1/T$ (K^{-1}) showed a linear fitting. The entropy change, ΔS°, and enthalpy change, ΔH°, were obtained from the slope and intercept of a plot of eq 5, while the Gibb's free energy change, ΔG°, could be calculated from eq 4. Since both ΔG° and ΔH° showed negative values, it is clear that the adsorption process of CTX onto MMO is a spontaneous exothermic process.[64,65]

3.2.5. Recyclability of ZnCoFe MMO for CTX Adsorption. The recycling of the used adsorbent for the successive adsorption of CTX was conducted and the results are shown in Figure 8. It is of importance to investigate the reusability performance of the MMO to minimize the costs of MMO utilization as the adsorbent. As shown at Figure 8, the removal

https://doi.org/10.1021/acsomega.2c05528
ACS Omega 2022, 7, 44103−44115

Table 4. Kinetic Study Model Fitting Parameters

model	equation	parameters	values
pseudo-first order	$q_t = q_e\,(1 - e^{-K_1 t})$, q_e is the adsorption capacity at equilibrium, K_1 is the pseudo-first-order rate constant	K_1 (min^{-1})	7.39×10^{-2}
		q_e (mg/g)	15.79
		R^2	0.98
pseudo-second order	$q_t = \frac{{q_e}^2 K_2 t}{1 + q_e K_2 t}$, K_2 is the pseudo-second-order rate constant	K_2 (g/(mg min))	0.62×10^{-2}
		q_e (mg/g)	17.7
		R^2	0.99
intraparticle diffusion	$q_t = K_{ip}\sqrt{t} + C_{ip}$, k_{ip} is the measure of diffusion coefficient, C_{ip} is the intraparticle diffusion constant	K_{ip} (mg/g $min^{0.5}$)	1.79
		C_{ip} (mg/g)	0.57
		R^2	0.96
Mixed first and second order	$q_t = q_e \frac{1 - e^{-K t}}{1 - f_2\, e^{-K t}}$, f_2 is the mixed 1,2 order coefficient and K is the adsorption rate constant	K (min^{-1})	0.18×10^{-2}
		q_e (mg/g)	17.5
		f_2 (g/(mg min))	0.98
		R^2	0.99
Avrami model	$q_t = q_e\,(1 - [e^{-K_{av} t}]^{n_{av}})$, K_{av} is the Avrami rate constant and n_{av} is the Avrami component	K_{av} (min^{-1})	0.28
		n_{av} (−)	0.26
		q_e (mg/g)	15.7
		R^2	0.99

Table 5. Thermodynamic Parameters for the CTX Adsorption Process onto MMO

material	T (K)	$\Delta G°$(kJ/mol)	$\Delta H°$(kJ/mol)	$\Delta S°$(J/mol K)
ZnCoFe MMO	298	−3.0	−2.6	63.07
	308	−3.4		
	318	−2.9		
	328	−0.96		

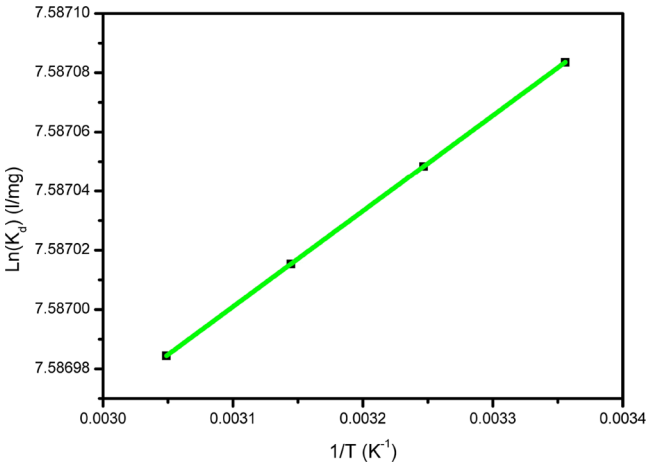

Figure 7. Plot of $\ln(K_d)$ versus inverted temperature, $1/T$ (K^{-1}).

amount of MMO for CTX decreased to 50% after five cycles. This decrease after several cycles was attributed to the loss of MMO material during the successive adsorption and regeneration cycles.[9] The recycle studies recommend that the used material has potential for CTX removal from wastewater. We can overcome this problem by supporting the powdered particles on a membrane for instance to decrease the loss of the used material with successive adsorption and regeneration.

3.3. Reusing ZnCoFe Spent MMO for MG Dye Removal. For the kinetic investigation, 50 mL of 100 mg/L MG solution was used with a MMO and MMO/CTX with a dose of 0.05 g at pH 7, and the concentration of MG was measured at time intervals from 2 to 120 min. To obtain a better explanation of the removal kinetics and to quantify the collected adsorption data, five kinetic models were applied to

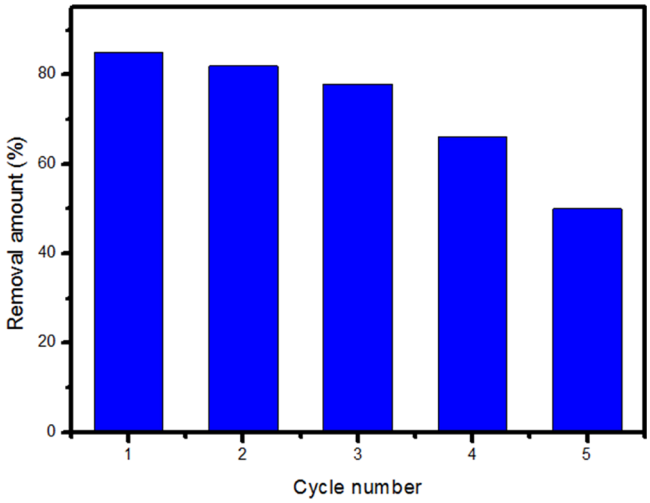

Figure 8. Recyclability of ZnCoFe MMO for CTX adsorption.

fit the experimental adsorption data. Figure 9 shows the experimental kinetic data together with the curves obtained from the kinetic models. Table 6 lists the fitting parameters for the used kinetic models. The experimental kinetic data showed rapid uptake for MG within the first 20 min followed by slow removal till equilibrium at 60 min, and then it was stable up to 120 min. Based on the correlation coefficient R^2, it has been proven that both pseudo-first-order and 1,2 mixed order are the best fit kinetic models with R^2 close to unity for both models. The calculated q_e ($q(e,\mathrm{cal})$) is 9.22 and 11.46 mg/g for the pseudo-first-order and 1,2 mixed order, respectively, which are very close to the equilibrium experimental one ($q(e,\mathrm{exp})$ = -----). At equilibrium, the spent adsorbent showed a removal percent of 94% for MG as opposed to 90% for the fresh ZnCoFe MMO. The possible mechanism of adsorption of MG in both cases is further discussed in the next section.

3.4. Adsorption Mechanism. CTX and ZnCoFe MMO can interact in different ways. One of which is the possible interaction of positive cations (Zn, Co, and Fe) in the tetrahedral position of the MMO layer with atoms having lone electron pair in CTX as shown in Figure 10a. Another possible interaction pathway is the hydrogen bonding between

https://doi.org/10.1021/acsomega.2c05528
ACS Omega 2022, 7, 44103−44115

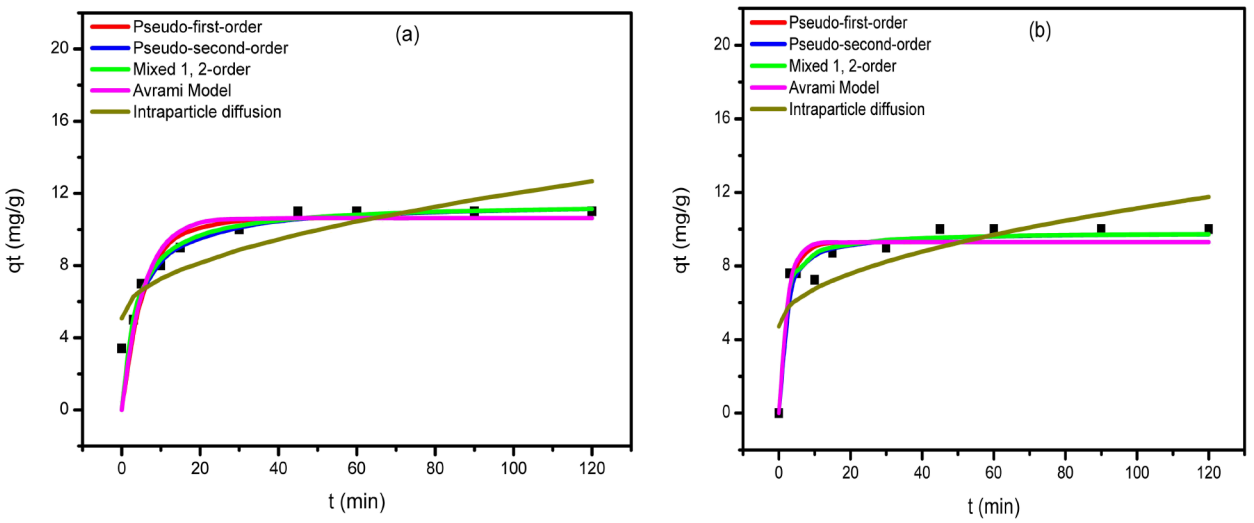

Figure 9. Adsorption kinetics of (a) ZnCoFe MMO/ MG and (b) ZnCoFe MMO/CTX/MG.

Table 6. Kinetic Study Model Fitting Parameters of MMO/MG and MMO/CTX/MG Samples

model	equation	parameters	MMO + MG	MMO/CTX + MG
pseudo-first order	$q_t = q_e\ (1 - e^{-K_1 t})$, q_e is the adsorption capacity at equilibrium and K_1 is the pseudo-first-order rate constant	K_1 (min^{-1})	18.65×10^4	18.64×10^4
		q_e (mg/g)	9.22	8.9
		R^2	0.86	0.96
pseudo-second order	$q_t = \frac{q_e^2 K_2 t}{1 + q_e K_2 t}$, K_2 is the pseudo-second-order rate constant	K_2 (g/(mg min))	1.03×10^6	1.03×10^6
		q_e (mg/g)	9.22	8.9
		R^2	0.83	0.96
intraparticle diffusion	$q_t = K_{ip}\sqrt{t} + C_{ip}$, K_{ip} is the measure of diffusion coefficient and C_{ip} is the intraparticle diffusion constant	K_{ip} (mg/g $min^{0.5}$)	0.69	0.64
		C_{ip} (mg/g)	5.07	4.71
		R^2	0.8	0.57
mixed first and second order	$q_t = q_e \frac{1 - e^{-K t}}{1 - f_2\ e^{-K t}}$, f_2 is the mixed 1,2 order coefficient and K is the adsorption rate constant	K (min^{-1})	12.82×10^{-4}	13.15×10^{-4}
		q_e (mg/g)	11.46	9.82
		f_2 (g/(mg min))	0.99	0.99
		R^2	0.97	0.99
Avrami model	$q_t = q_e\ (1 - [e^{-K_{av} t}]^{n_{av}})$, K_{av} is the Avrami rate constant and n_{av} is the Avrami component	K_{av} (min^{-1})	10.63	9.3
		n_{av} (−)	0.44	0.68
		q_e (mg/g)	0.41	0.65
		R^2	0.96	0.98

hydrogen atoms and oxygen on the surface of the MMO layer.[66] On the other hand, MG adsorption on ZnCoFe MMO can be attributed to the hydrogen bonding between the nitrogen atoms in MG and the surface hydroxyl groups on the MMO layers in solution as shown in Figure 10b.[67] When reusing MMO/CTX for the adsorption of MG, it is possible that the positive nitrogen center in MG is electrostatically attracted to partial negative centers in CTX in addition to possible hydrogen bonding with terminal oxygen groups as shown in Figure 10c. Figure 10d shows the FTIR spectra of MMO/CTX and MMO/CTX/MG. The peak at 1644 cm^{-1} corresponds to the stretching of the N−H group of the CTX molecule.[68−70] No extra peaks in the MMO/CTX/MG spectra reflected the formation of chemical bonds suggesting dominant physical interaction between CTX and MG.

3.5. Antimicrobial Study of ZnCoFe MMO. The MIC, minimum bactericidal concentration (MBC), and well diffusion assay were used to evaluate the antibacterial activity using different concentrations of ZnFeCo MMO. Figure 11 shows that the tested substance (ZnFeCo MMO) is effective in inhibiting the growth of both *S. aureus* and *E. coli*, but the bacteria most sensitive to this substance were Gram-positive bacteria, which had the largest inhibition zone compared to Gram-negative bacteria.

The results of the MIC and MBC also showed the effectiveness of the tested substance (ZnFeCo MMO) in inhibiting the growth of tested Gram-positive and negative bacteria at very low concentrations. The MIC and MBC for *S. aureus* were 5 and 10 mg/mL, respectively, while for *E. coli* it was 10 and 20 mg/mL, respectively. This indicates the intensity of the effectiveness of this substance as an antimicrobial. The findings of this study demonstrated that reactive oxygen species generated in the LDH metal content harmed proteins, DNA, and the cell membrane.

4. CONCLUSIONS

In this work, spent adsorbent valorization by further reuse for adsorption was investigated. A ZnCoFe MMO 2D nano-adsorbent was prepared by a simple co-precipitation technique. The MMO was characterized by XRD, FTIR, and SEM.

https://doi.org/10.1021/acsomega.2c05528
ACS Omega 2022, 7, 44103−44115

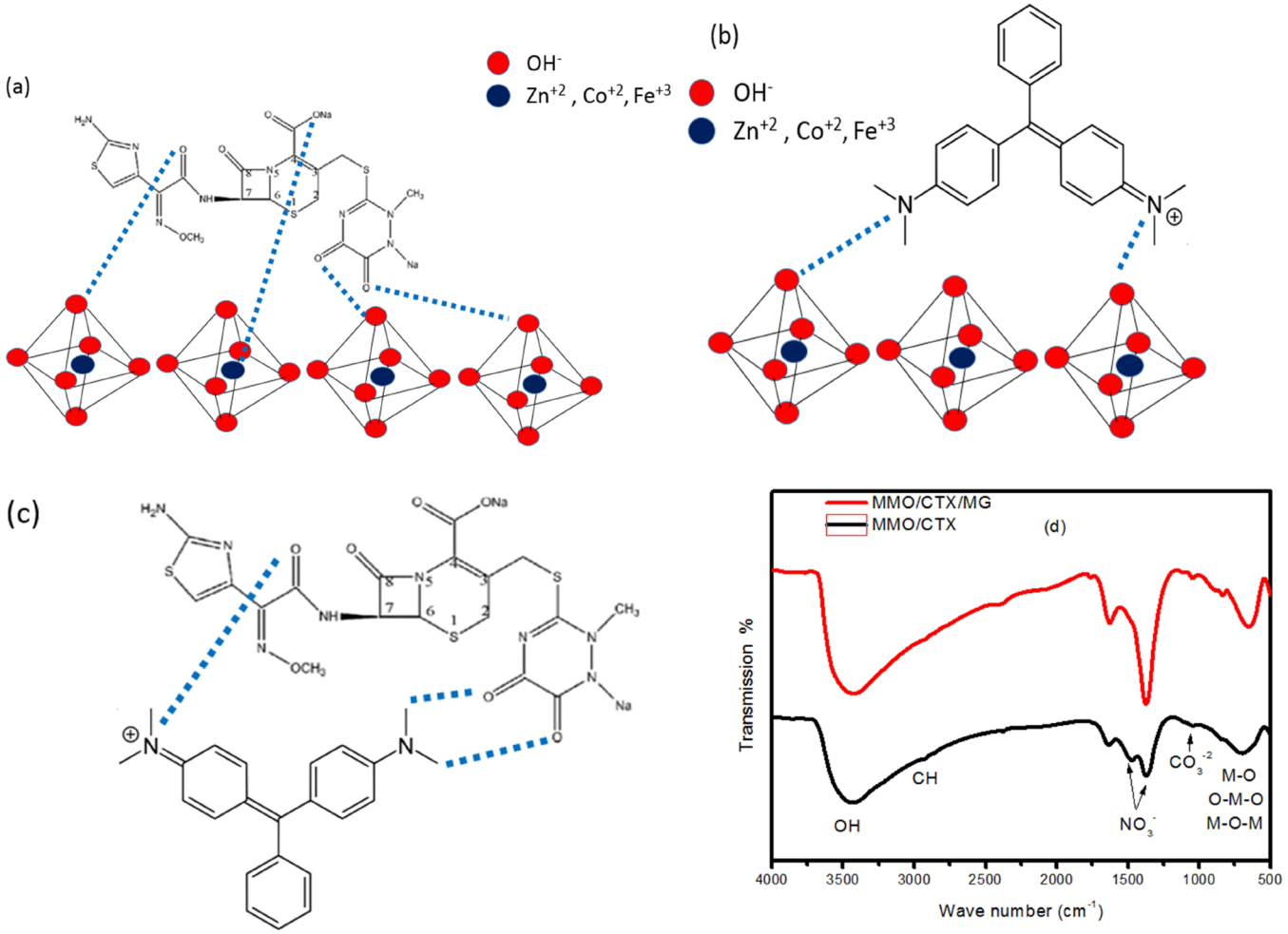

Figure 10. Possible adsorption mechanisms between (a) CTX and ZnCoFe MMO, (b) MG and ZnCoFe MMO, and (c) CTX and MG, and (d) FTIR of the samples MMO/CTX and MMO/CTX/MG.

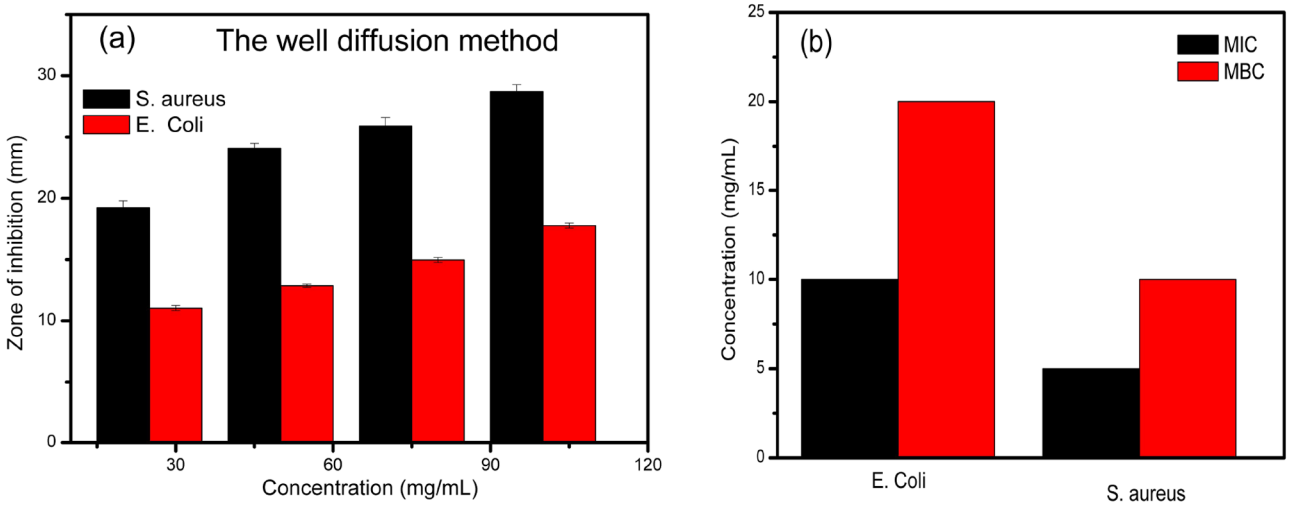

Figure 11. (a) Zone of inhibition and (b) MIC and MBC measurements of ZnCoFe MMO against Gram-positive and Gram-negative bacteria.

Adsorption equilibrium and kinetics for CTX adsorption on the ZnCoFe MMO were investigated. The spent adsorbent was further reused for MG adsorption. The spend adsorbent showed 94% removal percent for MG as compared to 90% for the as prepared fresh adsorbent. This study indicates the promising route of considering spent adsorbents for further adsorption of contaminants as an approach for waste valorization.

https://doi.org/10.1021/acsomega.2c05528
ACS Omega 2022, 7, 44103−44115

AUTHOR INFORMATION

Corresponding Author

Rehab K. Mahmoud − *Chemistry Department, Faculty of Sciences, Beni-Suef University, Beni-Suef 62511, Egypt;* orcid.org/0000-0002-1090-7445; Email: prof.rehab.mahmoud@gmail.com

Authors

Yasser GadelHak − *Department of Materials Science and Nanotechnology, Faculty of Postgraduate Studies for Advanced Sciences, Beni-Suef University, Beni-Suef 62511, Egypt;* orcid.org/0000-0001-5186-160X

Esraa Salama − *Chemistry Department, Faculty of Sciences, Beni-Suef University, Beni-Suef 62511, Egypt*

Samah Abd-El Tawab − *Food Science and Technology Department, Faculty of Agriculture, Fayoum University, Fayoum 63514, Egypt*

Eman Abouzied Mouhmed − *Food Science and Technology Department, Faculty of Agriculture, Fayoum University, Fayoum 63514, Egypt*

Dalal Hussien M. Alkhalifah − *Department of Biology, College of Science, Princess Nourah bint Abdulrahman University, Riyadh 11671, Saudi Arabia*

Wael N. Hozzein − *Botany and Microbiology Department, Faculty of Science, Beni-Suef University, Beni-Suef 62511, Egypt*

Mona Mohaseb − *Physics Department, Faculty of Science, Beni-Suef University, Beni-Suef 62511, Egypt; Department of Physics, Faculty of Applied Sciences, Umm-Al-Qura University, Mecca 21421, Saudi Arabia*

Rafat M. Amin − *Physics Department, Faculty of Science, Beni-Suef University, Beni-Suef 62511, Egypt*

Complete contact information is available at: https://pubs.acs.org/10.1021/acsomega.2c05528

Notes

The authors declare no competing financial interest.

ACKNOWLEDGMENTS

The authors acknowledge the support from Princess Nourah bint Abdulrahman University Researchers Supporting Project number (PNURSP2022R15), Princess Nourah bint Abdulrahman University, Riyadh, Saudi Arabia.

REFERENCES

(1) Iezzi, L.; Vilardi, G.; Saviano, G.; Stoller, M. On the Equipment Design of a Spinning Disk Reactor for the Production of Novel Nano Silver in Amorphous Zeolite Particles. *Chem. Eng. J.* **2022**, *449*, No. 137864.

(2) Acevedo-García, V.; Rosales, E.; Puga, A.; Pazos, M.; Sanromán, M. A. Synthesis and Use of Efficient Adsorbents under the Principles of Circular Economy: Waste Valorisation and Electroadvanced Oxidation Process Regeneration. *Sep. Purif. Technol.* **2020**, *242*, No. 116796.

(3) Baskar, A. V.; Bolan, N.; Hoang, S. A.; Sooriyakumar, P.; Kumar, M.; Singh, L.; Jasemizad, T.; Padhye, L. P.; Singh, G.; Vinu, A.; Sarkar, B.; Kirkham, M. B.; Rinklebe, J.; Wang, S.; Wang, H.; Balasubramanian, R.; Siddique, K. H. M. Recovery, Regeneration and Sustainable Management of Spent Adsorbents from Wastewater Treatment Streams: A Review. *Sci. Total Environ.* **2022**, *822*, No. 153555.

(4) Rial, J. B.; Ferreira, M. L. Potential Applications of Spent Adsorbents and Catalysts: Re-Valorization of Waste. *Sci. Total Environ.* **2022**, *823*, No. 153370.

(5) Mahmoud, R.; Safwat, N.; Fathy, M.; Mohamed, N. A.; El-Dek, S.; El-Banna, H. A.; Farghali, A.; Abo El-Ela, F. I. Novel Anti-Inflammatory and Wound Healing Controlled Released LDH-Curcumin Nanocomposite via Intramuscular Implantation, in-Vivo Study. *Arab. J. Chem.* **2022**, *15*, No. 103646.

(6) Mahmoud, R. K.; Taha, M.; Zaher, A.; Amin, R. M. Understanding the Physicochemical Properties of Zn−Fe LDH Nanostructure as Sorbent Material for Removing of Anionic and Cationic Dyes Mixture. *Sci. Rep.* **2021**, *11*, 21365.

(7) Laipan, M.; Fu, H.; Zhu, R.; Sun, L.; Zhu, J.; He, H. Converting Spent Cu/Fe Layered Double Hydroxide into Cr(VI) Reductant and Porous Carbon Material. *Sci. Rep.* **2017**, *7*, 7277.

(8) Shen, X.; Zhu, Z.; Zhang, H.; Di, G.; Chen, T.; Qiu, Y.; Yin, D. Carbonaceous Composite Materials from Calcination of Azo Dye-Adsorbed Layered Double Hydroxide with Enhanced Photocatalytic Efficiency for Removal of Ibuprofen in Water. *Environ. Sci. Eur.* **2020**, *32*, 77.

(9) Awes, H.; Zaki, Z.; Abbas, S.; Dessoukii, H.; Zaher, A.; Abd-El Moaty, S. A.; Shehata, N.; Farghali, A.; Mahmoud, R. K. Removal of Cu2+ Metal Ions from Water Using Mg-Fe Layered Double Hydroxide and Mg-Fe LDH/5-(3-Nitrophenyllazo)-6-Aminouracil Nanocomposite for Enhancing Adsorption Properties. *Environ. Sci. Pollut. Res.* **2021**, *28*, 47651−47667.

(10) Moustafa, D.; Mahmoud, R.; El-Salam, H. M. A.; Shehata, N. Utilization of Residual Zinc−Iron-Layered Double Hydroxide after Methyl Orange Management as a New Sorbent for Wastewater Treatment. *Appl. Nanosci.* **2021**, *11*, 709−723.

(11) Abdel-Hady, E. E.; Mahmoud, R.; Hafez, S. H. M.; Mohamed, H. F. M. Hierarchical Ternary ZnCoFe Layered Double Hydroxide as Efficient Adsorbent and Catalyst for Methanol Electrooxidation. *J. Mater. Res. Technol.* **2022**, *17*, 1922−1941.

(12) Mahmoud, M. E.; El-Ghanam, A. M.; Mohamed, R. H. A.; Saad, S. R. Enhanced Adsorption of Levofloxacin and Ceftriaxone Antibiotics from Water by Assembled Composite of Nanotitanium Oxide/Chitosan/Nano-Bentonite. *Mater. Sci. Eng. C* **2020**, *108*, No. 110199.

(13) Bozorginia, S.; Jaafari, J.; Taghavi, K.; Ashrafi, S. D.; Roohbakhsh, E.; Naghipour, D. Biosorption of Ceftriaxone Antibiotic by Pseudomonas Putida from Aqueous Solutions. *Int. J. Environ. Anal. Chem.* **2021**, 1−15.

(14) Shi, X.; Karachi, A.; Hosseini, M.; Yazd, M. S.; Kamyab, H.; Ebrahimi, M.; Parsaee, Z. Ultrasound Wave Assisted Removal of Ceftriaxone Sodium in Aqueous Media with Novel Nano Composite G-C3N4/MWCNT/Bi2WO6 Based on CCD-RSM Model. *Ultrason. Sonochem.* **2020**, *68*, 104460.

(15) Badi, M. Y.; Azari, A.; Pasalari, H.; Esrafili, A.; Farzadkia, M. Modification of Activated Carbon with Magnetic Fe3O4 Nanoparticle Composite for Removal of Ceftriaxone from Aquatic Solutions. *J. Mol. Liq.* **2018**, *261*, 146−154.

(16) Badri, A. F.; Siregar, P. M. S. B. N.; Palapa, N. R.; Mohadi, R.; Mardiyanto, M.; Lesbani, A. Mg-Al/Biochar Composite with Stable Structure for Malachite Green Adsorption from Aqueous Solutions. *Bull. Chem. React. Eng. Catal.* **2021**, *16*, 149−160.

(17) Baytar, O.; Ceyhan, A. A.; Şahin, Ö. Production of Activated Carbon from Elaeagnus Angustifolia Seeds Using H3PO4 Activator and Methylene Blue and Malachite Green Adsorption. *Int. J. Phytoremediation* **2021**, *23*, 693−703.

(18) Delpiano, G. R.; Tocco, D.; Medda, L.; Magner, E.; Salis, A. Adsorption of Malachite Green and Alizarin Red s Dyes Using Fe-Btc Metal Organic Framework as Adsorbent. *Int. J. Mol. Sci.* **2021**, *22*, 788.

(19) Zhang, T.; Jin, X.; Owens, G.; Chen, Z. Remediation of Malachite Green in Wastewater by ZIF-8@Fe/Ni Nanoparticles Based on Adsorption and Reduction. *J. Colloid Interface Sci.* **2021**, *594*, 398−408.

(20) *No Title*. https://pubchem.ncbi.nlm.nih.gov//edit3/index.html.

(21) *No Title*. https://www.chemspider.com/Chemical-Structure.21111741.html?rid=818d2cb2-4e42-4ddb-8e83-c44ecef53c69&page_num=0.

https://doi.org/10.1021/acsomega.2c05528
ACS Omega 2022, 7, 44103−44115

(22) *No Title*. https://www.chemicalbook.com/ChemicalProductProperty_EN_CB3350760.htm.
(23) *No Title*. https://pubchem.ncbi.nlm.nih.gov/compound/Ceftriaxone-sodium.
(24) Sayed, H.; Mahmoud, R.; Mohamed, H. F. M.; Gaber, Y.; Shehata, N.Co and Ni Double Substituted Zn-Fe Layered Double Hydroxide as 2D Nano-Adsorbent for Wastewater Treatment. In *Key Engineering Materials*; Trans Tech Publ2022, *922*, 193 −213.
(25) Gürses, A.; Doğar, Ç.; Yalçın, M.; Açıkyıldız, M.; Bayrak, R.; Karaca, S. The Adsorption Kinetics of the Cationic Dye, Methylene Blue, onto Clay. *J. Hazard. Mater.* **2006**, *131*, 217−228.
(26) Senthilkumaar, S.; Varadarajan, P. R.; Porkodi, K.; Subbhuraam, C. V. Adsorption of Methylene Blue onto Jute Fiber Carbon: Kinetics and Equilibrium Studies. *J. Colloid Interface Sci.* **2005**, *284*, 78−82.
(27) Rudzinski, W.; Plazinski, W. Kinetics of Dyes Adsorption at the Solid− Solution Interfaces: A Theoretical Description Based on the Two-Step Kinetic Model. *Environ. Sci. Technol.* **2008**, *42*, 2470−2475.
(28) Avrami, M. Kinetics of Phase Change. III: Granulation, Phase Change and Microstructure. *J. Chem. Phys.* **1941**, *9*, 177−184.
(29) Kuri, V.; Madden, R. H.; Collins, M. A.*Lactic Acid Bacteria and Salmonellae from Mexican Pork Products: Characterization and Antagonism*. 1998, *PhD*.
(30) Daeschel, M. A.*Procedures to Detect Antimicrobial Activities of Microorganisms*. In Food biopreservatives of microbial origin; CRC Press, 2019; =57−80.
(31) Fernández-López, J.; Zhi, N.; Aleson-Carbonell, L.; Pérez-Alvarez, J. A.; Kuri, V. Antioxidant and Antibacterial Activities of Natural Extracts: Application in Beef Meatballs. *Meat Sci.* **2005**, *69*, 371−380.
(32) Kim, B. K.; Lee, D. Y.; Gwak, G. H.; Han, Y. S.; Oh, J. M. Zn-Fe Mixed Metal Oxides from Metal Hydroxide Precursor: Effect of Calcination Temperature on Phase Evolution, Porosity, and Catalytic Acidity. *J. Solid State Chem.* **2019**, *269*, 454−458.
(33) Pan, D.; Ge, S.; Zhao, J.; Shao, Q.; Guo, L.; Zhang, X.; Lin, J.; Xu, G.; Guo, Z. Synthesis, Characterization and Photocatalytic Activity of Mixed-Metal Oxides Derived from NiCoFe Ternary Layered Double Hydroxides. *Dalton Trans.* **2018**, *47*, 9765−9778.
(34) Park, Y. M.; Lee, D. H.; Lee, Y. J.; Roh, H. S.; Chung, C. H.; Wook Bae, J. Ordered Mesoporous Co 3 O 4 −Al 2 O 3 Binary Metal Oxides for CO Hydrogenation to Hydrocarbons: Synergy Effects of Phosphorus Modifier for an Enhanced Catalytic Activity and Stability. *ChemCatChem* **2019**, *11*, 1707−1721.
(35) Gopinath, A.; Kadirvelu, K. Preparation and Characterization of Mixed Metal Oxide ZnCo2O4 Spinel Coated ACF for Environmental Remediation. *Mater. Res. Express* **2019**, *6*, No. 046518.
(36) Chinh, V. D.; Hung, L. X.; Di Palma, L.; Hanh, V. T. H.; Vilardi, G. Effect of Carbon Nanotubes and Carbon Nanotubes/Gold Nanoparticles Composite on the Photocatalytic Activity of TiO2 and TiO2-SiO2. *Chem. Eng. Technol.* **2019**, *42*, 308−315.
(37) Ghalmi, Y.; Habelhames, F.; Sayah, A.; Bahloul, A.; Nessark, B.; Shalabi, M.; Nunzi, J. M. Capacitance Performance of NiO Thin Films Synthesized by Direct and Pulse Potentiostatic Methods. *Ionics* **2019**, *25*, 6025−6033.
(38) El-Shahawy, A. A. G.; Moaty, S. A. A.; Zaki, A. H.; Mohamed, N. A.; Gadelhak, Y.; Mahmoud, R. K.; Farghali, A. A. Prostate Cancer Cellular Uptake of Ternary Titanate Nanotubes/CuFe2O4/Zn-Fe Mixed Metal Oxides Nanocomposite. *Int. J. Nanomedicine* **2020**, *15*, 619−631.
(39) Chinh, V. D.; Bavasso, I.; Di Palma, L.; Felici, A. C.; Scarsella, M.; Vilardi, G.; Bracciale, M. P.; Van, N. T. Enhancing the Photocatalytic Activity of TiO2 and TiO2−SiO2 by Coupling with Graphene−Gold Nanocomposites. *J. Mater. Sci.: Mater. Electron.* **2021**, *32*, 5082−5093.
(40) Owens, H. M.; Dash, A. K. Ceftriaxone Sodium: Comprehensive Profile. *Profiles Drug Subst. Excip. Relat. Methodol.* **2003**, *30*, 21−57.
(41) Abbas, K. K.; AbdulkadhimAl-Ghaban, A. M. H.; Rdewi, E. H. Synthesis of a Novel ZnO/TiO2-Nanorod MXene Heterostructured Nanophotocatalyst for the Removal Pharmaceutical Ceftriaxone Sodium from Aqueous Solution under Simulated Sunlight. *J. Environ. Chem. Eng.* **2022**, *10*, No. 108111.
(42) Goyal, M.; Singh, S.; Bansal, R. C. Equilibrium and Dynamic Adsorption of Methylene Blue from Aqueous Solutions by Surface Modified Activated Carbons. *Carbon Lett.* **2004**, *5*, 170−179.
(43) Ado, A. D.; Muhammad, M.; Mahmud, A. D.; Oyegoke, T. Adsorptive Removal of Chromium from Simulated Industrial Wastewater Using Kaolin-Based Adsorbent. *Trends Food Sci. Technol.* **2019**, *4*, 617−620.
(44) Ren, X.; Li, J.; Chen, C.; Gao, Y.; Chen, D.; Su, M.; Alsaedi, A.; Hayat, T. Graphene Analogues in Aquatic Environments and Porous Media: Dispersion, Aggregation, Deposition and Transformation. *Environ. Sci. Nano* **2018**, *5*, 1298−1340.
(45) Ren, X.; Li, J.; Chen, C.; Gao, Y.; Chen, D.; Su, M.; Alsaedi, A.; Hayat, T. Correction: Graphene Analogues in Aquatic Environments and Porous Media: Dispersion, Aggregation, Deposition and Transformation. *Environ. Sci. Nano* **2018**, *5*, 1518.
(46) Wu, L.; Liu, L.; Gao, B.; Muñoz-Carpena, R.; Zhang, M.; Chen, H.; Zhou, Z.; Wang, H. Aggregation Kinetics of Graphene Oxides in Aqueous Solutions: Experiments, Mechanisms, and Modeling. *Langmuir* **2013**, *29*, 15174−15181.
(47) Hotze, E. M.; Phenrat, T.; Lowry, G. V. Nanoparticle Aggregation: Challenges to Understanding Transport and Reactivity in the Environment. *J. Environ. Qual.* **2010**, *39*, 1909−1924.
(48) Langmuir, I. The Adsorption of Gases on Plane Surfaces of Glass, Mica and Platinum. *J. Am. Chem. Soc.* **1918**, *40*, 1361−1403.
(49) Nagy, B.; Mânzatu, C.; Măicăneanu, A.; Indolean, C.; Barbu-Tudoran, L.; Majdik, C. Linear and Nonlinear Regression Analysis for Heavy Metals Removal Using Agaricus Bisporus Macrofungus. *Arab. J. Chem.* **2017**, *10*, S3569−S3579.
(50) Dubinin, M. M. The Potential Theory of Adsorption of Gases and Vapors for Adsorbents with Energetically Nonuniform Surfaces. *Chem. Rev.* **1960**, *60*, 235−241.
(51) Sips, R. Combined Form of Langmuir and Freundlich Equations. *J. Chem. Phys* **1948**, *16*, 490−495.
(52) Redlich, O.; Peterson, D. L. A Useful Adsorption Isotherm. *J. Phys. Chem.* **1959**, *63*, 1024.
(53) Vilela, P. B.; Dalalibera, A.; Duminelli, E. C.; Becegato, V. A.; Paulino, A. T. Adsorption and Removal of Chromium (VI) Contained in Aqueous Solutions Using a Chitosan-Based Hydrogel. *Environ. Sci. Pollut. Res.* **2019**, *26*, 28481−28489.
(54) Toth, J. State Equation of the Solid-Gas Interface Layers. *Acta Chim. Hung.* **1971**, *69*, 311−328.
(55) Baudu, M.*Etude Des Interactions Solutes-Fibres de Charbon Actif: Applications et Regeneration*; Rennes 11990.
(56) Duman, O.; Polat, T. G.; Diker, C. Ö.; Tunç, S. Agar/κ-Carrageenan Composite Hydrogel Adsorbent for the Removal of Methylene Blue from Water. *Int. J. Biol. Macromol.* **2020**, *160*, 823−835.
(57) Duman, O.; Özcan, C.; Gürkan Polat, T.; Tunç, S. Carbon Nanotube-Based Magnetic and Non-Magnetic Adsorbents for the High-Efficiency Removal of Diquat Dibromide Herbicide from Water: OMWCNT, OMWCNT-Fe3O4 and OMWCNT-K-Carrageenan-Fe3O4 Nanocomposites. *Environ. Pollut.* **2019**, *244*, 723−732.
(58) Duman, O.; Tunç, S.; Bozoğlan, B. K.; Polat, T. G. Removal of Triphenylmethane and Reactive Azo Dyes from Aqueous Solution by Magnetic Carbon Nanotube-κ-Carrageenan-Fe3O4nanocomposite. *J. Alloys Compd.* **2016**, *687*, 370−383.
(59) Ho, Y. S.; McKay, G. Pseudo-Second Order Model for Sorption Processes. *Process Biochem.* **1999**, *34*, 451−465.
(60) El-Reesh, G. Y. A.; Farghali, A. A.; Taha, M.; Mahmoud, R. K. Novel Synthesis of Ni/Fe Layered Double Hydroxides Using Urea and Glycerol and Their Enhanced Adsorption Behavior for Cr (VI) Removal. *Sci. Rep.* **2020**, *10*, 587.
(61) Vinod, V. P.; Anirudhan, T. S. Sorption of Tannic Acid on Zirconium Pillared Clay. *J. Chem. Technol. Biotechnol.* **2002**, *77*, 92−101.

https://doi.org/10.1021/acsomega.2c05528
ACS Omega 2022, 7, 44103−44115

(62) Horsfall Jnr, M.; Spiff, A. Effect of Temperature on the Sorption of Pb2+ and Cd2+ from Aqueous Solution by Caladium Bicolor (Wild Cocoyam) Biomass. *Electron. J. Biotechnol.* **2005**, *8*, 162−169.
(63) Sarin, V.; Singh, T. S.; Pant, K. K. Thermodynamic and Breakthrough Column Studies for the Selective Sorption of Chromium from Industrial Effluent on Activated Eucalyptus Bark. *Bioresour. Technol.* **2006**, *97*, 1986−1993.
(64) Sepehr, M. N.; Al-Musawi, T. J.; Ghahramani, E.; Kazemian, H.; Zarrabi, M. Adsorption Performance of Magnesium/Aluminum Layered Double Hydroxide Nanoparticles for Metronidazole from Aqueous Solution. *Arab. J. Chem.* **2017**, *10*, 611−623.
(65) Elwakeel, K. Z.; Atia, A. A.; Guibal, E. Fast Removal of Uranium from Aqueous Solutions Using Tetraethylenepentamine Modified Magnetic Chitosan Resin. *Bioresour. Technol.* **2014**, *160*, 107−114.
(66) Rashidi Nodeh, H.; Sereshti, H. Synthesis of Magnetic Graphene Oxide Doped with Strontium Titanium Trioxide Nanoparticles as a Nanocomposite for the Removal of Antibiotics from Aqueous Media. *RSC Adv.* **2016**, *6*, 89953−89965.
(67) George, G.; Saravanakumar, M. P. Facile Synthesis of Carbon-Coated Layered Double Hydroxide and Its Comparative Characterisation with Zn−Al LDH: Application on Crystal Violet and Malachite Green Dye Adsorption—Isotherm, Kinetics and Box-Behnken Design. *Environ. Sci. Pollut. Res.* **2018**, *25*, 30236−30254.
(68) Jamil, B.; Habib, H.; Abbasi, S. A.; Ihsan, A.; Nasir, H.; Imran, M. Development of Cefotaxime Impregnated Chitosan as Nano-Antibiotics: De Novo Strategy to Combat Biofilm Forming Multi-Drug Resistant Pathogens. *Front. Microbiol.* **2016**, *7*, 330.
(69) Singh, D.; Rathod, V.; Ninganagouda, S.; Hiremath, J.; Singh, A. K.; Mathew, J. Optimization and Characterization of Silver Nanoparticle by Endophytic Fungi Penicillium Sp. Isolated from Curcuma Longa (Turmeric) and Application Studies against MDR E. Coli and S. Aureus. *Bioinorg. Chem. Appl.* **2014**, *2014*, No. 408021.
(70) Zhang, X. H.; Cao, D. M.; Zhao, S. Y.; Gong, P.; Hei, D. Q.; Zhang, H. Q. Gamma Radiolysis of Ceftriaxone Sodium for Water Treatment: Assessments of the Activity. *Water Sci. Technol.* **2011**, *63*, 2767−2774.

https://doi.org/10.1021/acsomega.2c05528
ACS Omega 2022, 7, 44103−44115